Structure and Mechanism of the Glycerol-3-Phosphate Transporter from *Escherichia coli*

Yafei Huang,* M. Joanne Lemieux,*† Jinmei Song, Manfred Auer, Da-Neng Wang‡

The major facilitator superfamily represents the largest group of secondary membrane transporters in the cell. Here we report the 3.3 angstrom resolution structure of a member of this superfamily, GlpT, which transports glycerol-3-phosphate into the cytoplasm and inorganic phosphate into the periplasm. The amino- and carboxyl-terminal halves of the protein exhibit a pseudo two-fold symmetry. Closed off to the periplasm, a centrally located substrate-translocation pore contains two arginines at its closed end, which comprise the substrate-binding site. Upon substrate binding, the protein adopts a more compact conformation. We propose that GlpT operates by a single–binding site, alternating-access mechanism through a rocker-switch type of movement.

Membrane transport in cells is a fundamental biological process that is mediated by various channel and transporter proteins. A major type of such proteins is secondary active membrane transporters, which use a solute gradient to drive the translocation of other substrates (*1*). The largest secondary transporter protein family known so far is the major facilitator superfamily (MFS) (*2*–*4*), with more than 1000 members identified to date (*5*). These proteins transport ions, sugars, sugar-phosphates, drugs, neurotransmitters, nucleosides, amino acids, peptides, and other hydrophilic solutes. Members of this superfamily are ubiquitous in all three kingdoms of living organisms, and many have medical or pharmacological relevance. For example, the mammalian glucose transporter Glut4 from muscle and adipose cells is responsible for their glucose uptake, a process that is impaired in type II diabetes (*6*). Mutations in a related transporter, Glut1 from erythrocyte and brain-blood barrier, cause glucose transporter 1 deficiency syndrome, a disease whose symptoms include infantile seizures and developmental delay (*7*). Similarly, mutations in human glucose-6-phosphate transporter (G6PT) cause glycogen storage disease type 1b (*8*). In bacteria, MFS proteins function principally for nutrient uptake [like *E. coli* lactose permease (LacY) (*9*)], but some act as drug-efflux pumps that confer antibiotic resistance (*10*).

MFS proteins are typically 400 to 600 amino acids long and share transmembrane topology similarities and signature sequences in two cytosolic loops. Hydropathy sequence analysis and reporter-fusion experiments indicate that most MFS proteins have 12 transmembrane α helices, with both the N- and C-termini located in the cytosol (*4*). The two six-helix halves of an MFS protein, connected by a long central loop, are related by weak sequence similarity (*11*). Structurally, the best-characterized MFS protein to date is the oxalate transporter (OxlT) from *Oxalobacter formigenes*. A 6.5 Å map of OxlT in a substrate-bound form determined by cryoelectron microscopy revealed 12 transmembrane α helices surrounding a central pore (*12*, *13*).

The substrate-translocation mechanism most commonly ascribed to secondary membrane transporters is the alternating-access mechanism that was developed on the basis of thermodynamic considerations and kinetic studies (*14*–*16*). In this mechanism, the transporter is believed to have two major alternating conformations: inward-facing (C_i) and outward-facing (C_o). At any moment, a single binding site in a polar cavity is accessible to only one side of the membrane. Interconversion between the two conformations in an antiporter is only possible via a substrate-bound form(s) of the protein. Many fundamental questions remain regarding the characteristics of the substrate-binding site, the coupling of the solute gradient with substrate transport, and the conformational changes required for the substrate translocation (*9*, *16*).

We attempted to address these questions by determining the crystal structure of an MFS protein. Using the strategies of searching crystallization space by cloning (*17*) and identifying flexible termini and tags by proteolysis and mass spectrometry (*18*), we crystallized GlpT, the glycerol-3-phosphate (G3P) transporter from the *E. coli* inner membrane, in the absence of a substrate (*19*). In *E. coli*, G3P serves both as a carbon and energy source and as a precursor for phospholipid biosynthesis (*20*, *21*). GlpT is an organic phosphate/inorganic phosphate (P_i) antiporter that functions for G3P uptake and is driven by a P_i gradient (*21*–*23*). In reconstituted systems, this transporter can also mediate P_i/P_i exchange. GlpT binds to substrates in detergent solution and, upon reconstitution into proteoliposomes, mediates G3P to P_i exchange (*24*). The protein is closely related to the *E. coli* hexose-6-phosphate transporter (UhpT) (*25*). Here we report the structure of GlpT at 3.3 Å resolution as

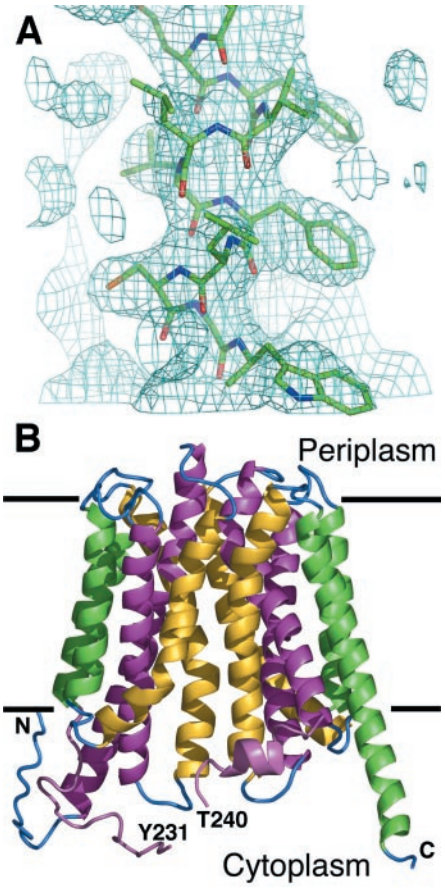

Fig. 1. Electron density map and overall structure of GlpT. (**A**) $2F_o - F_c$ map at 3.3 Å resolution, contoured at 1σ, shown together with a part of the GlpT model. (**B**) Ribbon representation of GlpT viewed from within the membrane. The GlpT molecule measures about 35 by 45 Å at the top and 35 by 60 Å at the bottom, and its height is about 60 Å. The final model contains sequences Phe^5 to Tyr^{231}, and Thr^{240} to Glu^{448}, in addition to the C-terminal Leu-Val-Pro sequence of the thrombin cleavage site. The figure was prepared with the program Pymol (*46*).

Skirball Institute of Biomolecular Medicine and Department of Cell Biology, New York University School of Medicine, 540 First Avenue, New York, NY 10016, USA.

*These authors contributed equally to this work.
†Present address: Department of Biochemistry, University of Alberta, Edmonton, Canada T6G 2H6.
‡To whom correspondence should be addressed. E-mail: wang@saturn.med.nyu.edu

determined by x-ray crystallography. The transporter structure suggests a mechanism for substrate translocation.

Structure determination. X-ray diffraction data were collected from a native, tungsten-cluster derivative and SeMet crystals (Table 1) (*26*). After solvent flattening and phase extension, experimental maps at 3.3 Å resolution showed 12 transmembrane α helices with the densities expected for aromatic side chains (Fig. 1A). The building and refinement of accurate atomic models were facilitated by locating selenomethionine residues in the anomalous difference maps from the SeMet crystals (fig. S1). The 12 helices are designated H1 to H12, and their connecting loops L1-2 to L11-12 (Fig. 1B).

Structure. The GlpT molecule has the shape of a Mayan temple, with a flat, rectangular top and bottom (Fig. 2) (fig. S1 and Movie S1). It can be divided into two similar domains, such that the N-terminal half is related to the C-terminal portion by a central pseudo two-fold symmetry axis perpendicular to the membrane plane (Fig. 2, A and B). Viewed along the membrane normal, this pseudo two-fold symmetry extends to all helices and most loops, with H1 related to H7, H2 to H8, and so forth. The domain interface is approximately perpendicular to the long axis of the molecule, where both polar and nonpolar residues are found. Looking from within the membrane plane along the domain interface (Fig. 1B), we observe a pore that is closed at one side of the membrane and open at the other (Fig. 2A). Because both the N- and C-termini are located in the cytosol (*27*), the pore opening faces the cytosolic side of the membrane. The position of the membrane-embedded portion of the molecule is inferred from the heights of the three shortest transmembrane α helices: H3, H6, and H9. It follows that the periplasmic side of the molecule is flat and protrudes only slightly into the periplasm (Figs. 1B and 2C). In contrast, several transmembrane α helices extend beyond the membrane surface on the cytoplasmic side. In both halves of the molecule, the helices form two three-helix bundles: H1-H5-H6 and H2-H3-H4 in the N-terminal domain, and H7-H11-H12 and H8-H9-H10 in the C-terminal domain. The two three-helix bundles in each domain are inserted into the membrane in opposite orientations (Fig. 2, A and B). Similar arrangements in helix orientation have been observed with other membrane proteins involved in transport (*28–30*). Whereas the observed pseudo two-fold symmetry between the domains is in agreement with the suggestion that MFS proteins arose by gene duplication (*11*), the arrangement of the helix bundle in each domain suggests that a gene-insertion event preceded the duplication.

The helix arrangements in GlpT can also be analyzed by their positions relative to the central pore (Fig. 2, A and B). Eight peripheral helices form a rectangular fence, which acts as a scaffold for the remaining four central helices. Whereas four of the peripheral helices, H3 and H6 in the N-terminal domain and H9 and H12 in the C-terminal domain, form the two narrow walls of the fence, the two wide walls are formed by H2 and H11 in the front, and H5 and H8 in the back. Because the latter four helices are curved into a banana-like shape, each pair has the shape of an hourglass, with the helices making contact in the membrane but being separated from each other in the cytosol (Fig. 1B and Movie S1). Both pairs are tilted about 20° from the membrane normal, but in opposite direc-

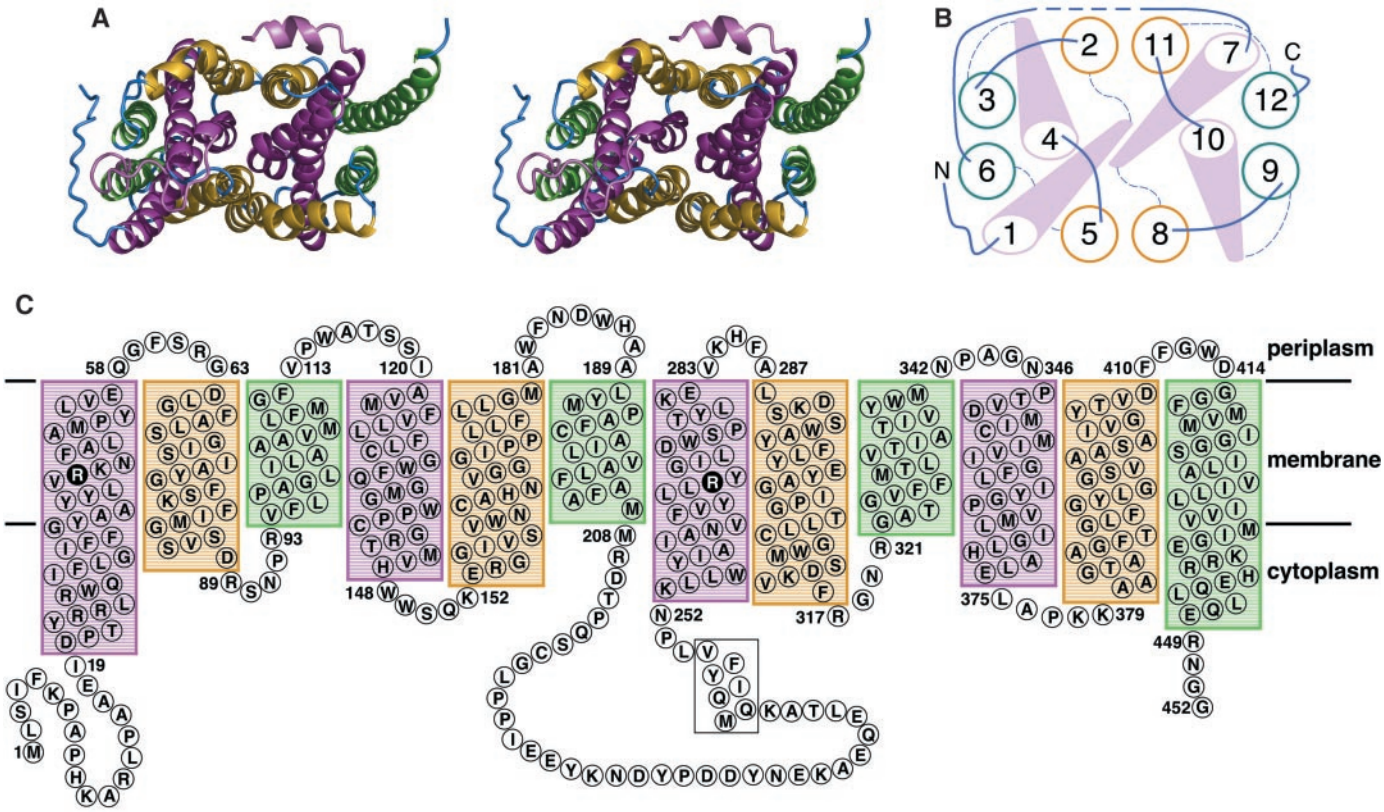

Fig. 2. GlpT structure. (**A**) Stereo view of a ribbon representation of GlpT viewed from the cytosol. Four peripheral helices (H3, H6, H9, and H12) that are not involved in pore formation are colored green, whereas the four that line the central pore (H2, H5, H8, and H11) are colored yellow. The four central helices (H1, H4, H7, and H10) are colored purple. The C-terminus of loop L6-7 forms a short helix that lies parallel to the membrane surface. (**B**) Schematic drawing showing the arrangements of transmembrane α helices viewed from the cytosol. The thick solid lines represent the loops on the cytosolic side, whereas the thin dashed lines represent the loops on the periplasmic side. The thick dashed line denotes the disordered segment in L6-7. (**C**) Wild-type amino acid sequence and transmembrane topology of GlpT. The N- and C-terminal halves of the protein have weak sequence homology. Residues Arg^{45} in H1 and Arg^{269} in H7 are indicated in the sequence. (A) was prepared with the program Pymol (*46*).

tions. Between the helices in each pair lies the interface of the N- and C-terminal domains. Into the rectangular fence formed by the above eight helices, two pairs of central helices insert from opposite sides of the membrane. H1 and H7 from the longer pair, which enter from the far sides of the molecule, tilt toward the center, and make close contact on the periplasmic side. The two shorter central helices, H4 and H10, transverse the diagonal of the respective narrow walls and make no contact with each other.

The N- and C-terminal domains are connected by a long central loop, L6-7 (45 amino acids long). The loop is partially disordered in our crystals, so residues from Asn^{232} to Leu^{239} are not visible in the structure (Figs. 1B and 2). The C-terminus of the central loop makes a two-turn helix that lies parallel to the membrane surface. It forms a helix-turn-helix motif with H7, surrounding the cytosolic end of H11 from the outside (Fig. 2A). Most of the remaining loops that connect transmembrane helices are five to six amino acids long, except for L5-6 and L3-4 (Fig. 2C). Part of L3-4 forms a short helix of 1.5 turns. As a result of being connected by such short loops, the helices in each six-helix domain are constrained from large-scale relative movement. On the cytosolic side of the molecule, two arginines in each of the two MFS signature sequences (*4*, *11*), RXXXR and RXXR, define the two ends of loops L2-3 and L8-9 (Fig. 2C). Similarly, cytoplasmic loop L10-11 contains two lysines. These positively charged residues probably help to position and orient the transmembrane helices when the protein undergoes membrane insertion, as observed for Glut1 (*31*). The change of the C-terminal arginine of L8-9 to a tryptophan is one of the mutations that cause human Glut1 deficiency syndrome (*7*).

Substrate-translocation pathway. GlpT purifies in a variety of detergents as a monomer that binds to substrates in solution (*24*). Its homolog, UhpT from *E. coli*, has been shown not only to purify as a monomer but also to function as one in the membrane (*32*). It is thus likely that GlpT functions as a monomer in the membrane as well. Therefore, the only plausible substrate-translocation pathway in our structure is the central pore at the interface of the N- and C-terminal domains (Figs. 2 and 3). Because the pore opens only to the cytosolic side, our structure represents GlpT in its inward-facing conformation in the absence of a substrate (C_i). On the other side of the protein, the periplasmic barrier is ~22 Å thick. The central part of the barrier is composed of portions of H1 and H7. The space between H1 and H7 is filled by nine aromatic side chains that help to close the pore completely. The role of these bulky side chains in pore closure partially explains the abundance of aromatic residues in the GlpT sequence (18%) and their even distribution across the transmembrane α helices (Fig. 2C), unlike other membrane proteins in which such residues typically form two aromatic belts on the membrane surfaces (*33*).

The substrate-translocation pore opens from the middle of the membrane (Fig. 3 and Movie S1). This pore is lined by four peripheral helices (H2 and H11 in front and H5 and H8 in the back) and four central helices (H1, H4, H7, and H10). It is about 30 Å deep and is divided into two regions: a funnel-shaped outer part and a cylindrical inner part. Viewed from the cytosol, the axis of the inner cylinder is tilted about 25° from the membrane normal toward the N-terminal half of the molecule. The axis of the funnel part, by contrast, is tilted by 25° toward the C-terminal half. The inner part of the pore measures 10 Å by 8 Å and has several amino acid side chains protruding into the pore. Its surface electrostatic potential is positive, particularly at the innermost end. The interior surface of the funnel, however, is mostly hydrophobic, except at its outermost extremities. This ensures that ions and water molecules do not adhere to the funnel surface. The cytoplasmic ends of helices H4 and H5, along with the connecting loop L4-5, and their partners in the C-terminal domain—H10, H11, and L10-11—form the outermost parts of the pore at two sides. The cytoplasmic ends of H1 and H7 make contact with L4-5 and L10-11, respectively, from outside (Fig. 2, A and B). Such a spatial arrangement between the two long central helices and these two loops may be optimal for transmitting substrate-induced conformational changes from the binding site to the rest of the protein (see below). Separating the inner and outer parts of the pore is

Table 1. Data collection, structure determination, and refinement. Numbers in parentheses are statistics of the highest resolution shell. NSLS, National Synchrotron Light Source; APS, Advanced Proton Source.

	Native*	W-cluster-GlpT	SeMet-GlpT
Beamline	X25 at NSLS	X25 at NSLS	19ID at APS
Wavelength (Å)	0.9789	1.214	0.9791
Resolution (Å)	20–3.3	20–3.9	20–4.0
Completeness (%)	99.5 (93.2)	98.9 (92.5)	100 (100)
R_{symm} (%)†	6.0 (38.6)	10.6 (32.7)	12.5 (28.9)
I/σ	11.3 (2.8)	11.0 (6.0)	5.6 (5.2)
Unique reflections	14,870	8,791	8,710
Redundancy‡	7.7 (4.3)	8.8 (7.5)	12.0 (12.0)
Phasing:			
R_{cullis} (acentric/centric)		0.779/0.846	
Phasing power (acentric/centric)		0.997/0.748	
Refinement:			
Resolution (Å)	15–3.3		
R_{work}/R_{free} (%)§	29.65/32.53		
Average *B* factor (Å^2)¶	84.2		
rmsd (bond/angle; Å/°)‖	0.0098/2.1		

*Space group: $P3_221$; unit cell: $a = b = 97.6$ Å, $c = 175.2$ Å, $\alpha = \beta = 90°$, $\gamma = 120°$. †$R_{symm} = \Sigma|I_j - \langle I_j \rangle|/\Sigma I_j$, where $\langle I_j \rangle$ is the averaged intensity for symmetry related reflections. ‡Redundancy represents the ratio between the number of measurements and the number of unique reflections. §R factor = $\Sigma|F(\text{obs}) - F(\text{calc})|/\Sigma F(\text{obs})$; 5% of the data that were excluded from the refinement were used to calculate R_{free}. ¶The average *B* factor was calculated for all nonhydrogen atoms. ‖rmsd of bond is the root-mean-square deviation of the bond angle and length.

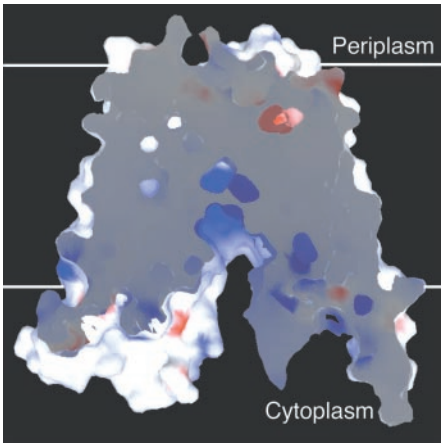

Fig. 3. Substrate-translocation pathway and periplasmic barrier. Electrostatic surface potential of GlpT is shown with the front part of the molecule removed for clarity. Blue indicates positive potential. The pathway is located in the interface between the N- and C-terminal domains. It opens in the middle of the membrane to the cytoplasmic side, but is closed off to the periplasm. The electrostatic surface potential is highly positive at the closed end of the translocation pathway. The figure was prepared with the program GRASP (*47*).

a protrusion on the N-terminal side that is formed by two tryptophans, Trp^{138} and Trp^{161}. On the opposite wall of the pore, a concave space is found in the C-terminal domain that has a shape complementary to that of the protrusion on the N-terminal domain (Fig. 3).

Substrate-binding site. Because substrate binding to GlpT is mediated by the phosphate moiety (*21*, *24*), which is dibasic at physiological pH, the substrate-binding site in GlpT is expected to have a positive surface electrostatic potential. The only area in the central pore with this characteristic is at the closed end of the pore in the middle of the membrane (Fig. 3). Thus, this area most likely represents the substrate-binding site.

There are two positively charged residues at the proposed substrate-binding site: Arg^{45} from H1 and Arg^{269} from H7 (Fig. 4 and fig. S2A). Located at an angle between these two arginines is His^{165} from H5. Whether this histidine is charged in such a basic environment is unclear. Another positively charged residue, Lys^{46}, is shielded from the pore by two tyrosines and thus cannot participate directly in substrate-binding in the C_i conformation. The two arginines and the histidine are conserved among bacterial GlpT and UhpT but not among other MFS proteins (fig. S2B). As a hydrogen donor, arginine residues often participate in phosphate recognition in proteins by forming hydrogen bonds with its oxygen atoms (*34*). Indeed, it has been shown that of the 14 arginine residues in *E. coli* UhpT, only the two that are equivalent to Arg^{45} and Arg^{269} of GlpT cannot be replaced by a lysine without destroying substrate transport activity (*35*). Arg^{45} and Arg^{269} in our structure are located at approximately the same height in the membrane. The conformational flexibility of their side chains is constrained in each case by five surrounding residues, mostly conserved and aromatic (Fig. 4B). The shortest distance between guanidinium groups of Arg^{45} and Arg^{269} is 9.9 Å, which may have important implications for the substrate-translocation mechanism of the transporter (see below). Mutations of the equivalent arginine of Arg^{45} in the human glucose-6-phosphate transporter to a cysteine or histidine cause glycogen storage disease type 1b (*8*).

Substrate-induced conformational change. We next investigated the conformational changes induced in GlpT upon substrate binding to its C_i state. Trypsin treatment of inside-out vesicles prepared from *E. coli* cells that expressed GlpT and of purified GlpT in detergent solution produced two protein fragments (fig. S3). Mass spectrometry measurements revealed the trypsin-sensitive site to be at Lys^{234}, located in the protein segment in L6-7 that is disordered in our crystal structure. The trypsin cleavage of GlpT, either membrane-bound or in detergent, was inhibited by the presence of G3P or P_i. Furthermore, the Stokes radius of GlpT in detergent solution was reduced from 42 to 40 Å upon the addition of G3P. These experiments suggest that GlpT changes to a more compact conformation when a substrate is bound.

Proposed transport mechanism. We propose that GlpT operates by a single–binding site, alternating-access mechanism (Fig. 5). In our structure, the shortest distance between the guanidinium groups of Arg^{45} and Arg^{269} is about 9.9 Å (Fig. 4B). For the oxygen atoms of the bound phosphate substrate to form hydrogen bonds of an optimal length (2.9 Å) (*36*) simultaneously with the guanidinium groups of both arginines, these two protein side chains must move 1.4 Å closer to each other (fig. S4). We propose that substrate binding pulls these two arginines on H1 and H7 closer. The movement of the two helices, transmitted via loops L4-5 and L10-11 (Fig. 2, A and B), brings the N- and

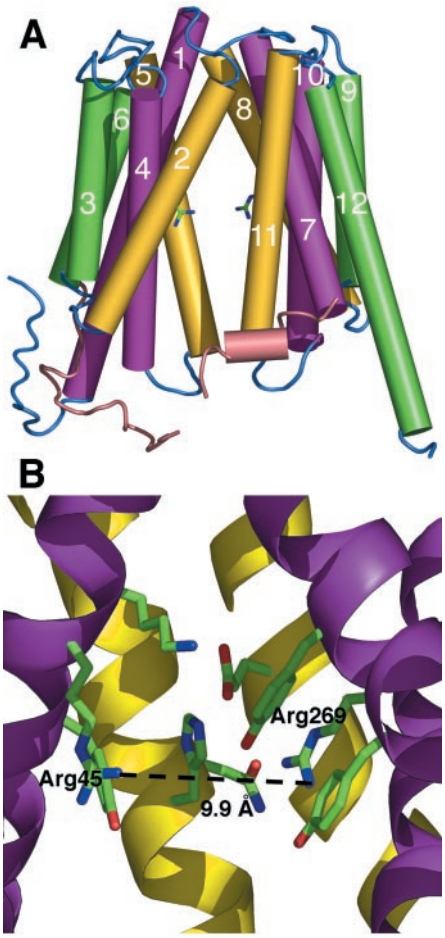

Fig. 4. Substrate-binding site. (**A**) The α helices are shown as straight cylinders with colors corresponding to those in Fig. 2. Arg^{45} from H1 and Arg^{269} from H7, key residues for substrate binding, are located at the closed end of the substrate-translocation pathway in the middle of the membrane. (**B**) Substrate-binding site. The shortest distance between guanidinium groups of Arg^{45} and Arg^{269} is 9.9 Å. The figure was prepared with the program Pymol (*46*).

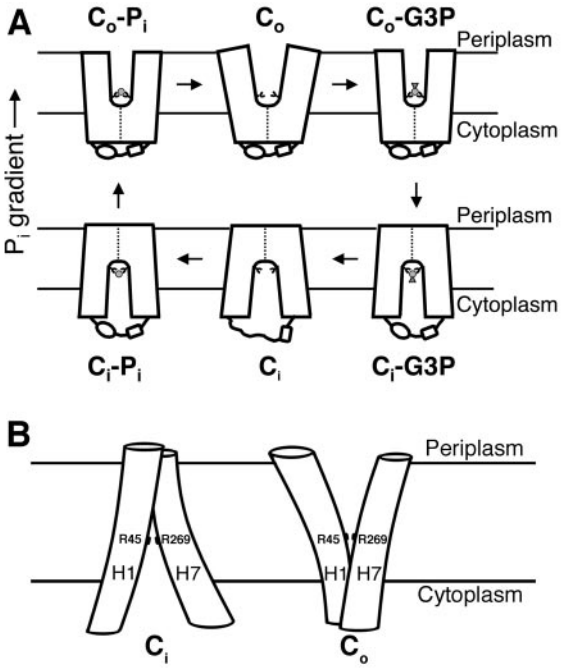

Fig. 5. Proposed single–binding site, alternating-access mechanism. Positions of Arg^{45} and Arg^{269} are indicated. (**A**) Reaction cycle of substrate translocation. P_i is represented by a small disk, and the G3P molecule by a small disk and a triangle. (**B**) Schematic drawing of central helices H1 and H7 in C_i and C_o conformations. Other helices are omitted for clarity. Rocker-switch–type movements of the helices that occur upon substrate binding allow the substrate-binding site, which comprises Arg^{45} and Arg^{269}, to switch between the two sides of the membrane.

C-terminal domains closer. This narrows the cytosolic pore and, at the same time, destabilizes the interface between the N- and C-terminal domains on the periplasmic side. Further tilting of N- and C-terminal domains relative to each other would close the central pore on the cytoplasmic side and open a new pore at the domain interface on the periplasmic side. This "rocker-switch" type of motion would expose the substrate-binding site, presumably still consisting of Arg^{45} and Arg^{269}, to the periplasm, yielding the outward-facing conformation (Fig. 5B). Periplasmic release of P_i would allow its replacement in the substrate-binding site by G3P, which has a higher affinity (*22*, *24*); on the cytoplasmic side of the membrane, P_i would replace G3P because of its higher cytosolic concentration. The two substrate-bound complexes for each substrate, C_i-S and C_o-S (S denotes substrate), are proposed to be similar energetically, which can most easily be achieved if the two states are structurally and functionally symmetrical. In summary, substrate binding is proposed to lower the energy barrier between the inward- and outward-facing conformations of GlpT, facilitating their interconversion and allowing the P_i gradient to drive G3P transport.

The rocker-switch type of conformational changes of GlpT proposed to accompany its substrate translocation can be understood from the transporter structure. In the C_i conformation, the interactions between the N- and C-terminal domains are relatively weak. Although there is extensive van de Waals contact between the domains at their interface, no salt bridge and few hydrogen bonds exist. At the interface, the convex curvature of the helices in each pair (H2/H11 and H5/H8) would enable a rocker-switch type of movement in which the periplasmic ends of these helices would separate as their cytoplasmic ends move closer together. Indeed, by separately rotating the two halves of our GlpT model (Figs. 1B and 4A) in opposite directions along an axis at the interface and parallel to the membrane, we found that a ~6° rotation by each domain can generate a structure similar to the substrate-bound form of OxlT (*12*). A ~10° rotation by each domain is sufficient to close the pore on the cytosolic side of the molecule and, at the same time, to open a pore on the periplasmic side (Movie S2). More importantly, the protrusion formed by Trp^{138} and Trp^{161} in the N-terminal domain would fit nicely into the complementary cavity on the C-terminal half of the protein (Fig. 3), thus closing the cytosolic pore in the C_o conformation. Certain movements of both the helices and their side chains within each domain, of course, are necessary for such a mechanism.

The proposed single–binding site, alternating-access mechanism (Fig. 5) is also supported by previous genetic, biochemical, and functional studies on other MFS proteins. Whole-cell experiments with UhpT show that residues equivalent to Leu^{288}, Thr^{278}, and Pro^{277} in H7 of GlpT (Fig. 2C) are accessible from the periplasmic side of UhpT in its C_o state, whereas the Tyr^{270} equivalent is only partially accessible (*37*). This again places Arg^{269} at the closed end of the pore in the C_o conformation of GlpT. Functional symmetry has been observed for UhpT, whose C_i and C_o states have similar substrate specificities (*38*). In addition, suppressor mutagenesis experiments on LacY suggest that a conserved aspartate at the cytoplasmic end of H2, equivalent to Asp^{88} of GlpT (Fig. 2C), interacts with H11 and plays a role in the C_i and C_o interconversion (*39*). This agrees with our proposal of the rocker-switch type of movement for the N- and C-terminal domains during substrate translocation. Finally, biochemical experiments suggest that glucose binding to Glut1 reduces the average tilt angle of its α helices (*40*), decreases the central pore size (*41*), and changes the susceptibility of L6-7 to proteolysis (*42*).

Our structure for GlpT is likely to be a paradigm for other MFS proteins, whose basic architecture is expected to be similar. Indeed, the overall helix arrangement in the 6.5 Å OxlT structure (*12*, *13*) and a LacY structural model based on biochemical data (*39*, *43*) resemble the GlpT structure. Substitution of a few key amino acid residues in the substrate-binding site of several MFS proteins could change the specificity of the transporter while retaining the single–binding site, alternating-access mechanism (*44*, *45*), thereby explaining the diverse substrate specificity for members of the major facilitator superfamily.

References and Notes

1. P. Mitchell, *Biochem. Soc. Symp.* **22**, 141 (1963).
2. J. Reizer *et al.*, *Protein Sci.* **2**, 20 (1993).
3. P. J. F. Henderson, *Curr. Opin. Cell Biol.* **5**, 708 (1993).
4. S. S. Pao, I. T. Paulsen, M. H. Saier Jr., *Microbiol. Mol. Biol. Rev.* **62**, 1 (1998).
5. www.membranetransport.org/.
6. B. B. Kahn, *J. Clin. Invest.* **89**, 1367 (1992).
7. D. Wang, P. Kranz-Eble, D. C. De Vivo, *Hum. Mutat.* **16**, 224 (2000).
8. L. Y. Chen, C. J. Pan, J. J. Shieh, J. Y. Chou, *Hum. Mol. Genet.* **11**, 3199 (2002).
9. H. R. Kaback, J. Wu, *Q. Rev. Biophys.* **30**, 333 (1997).
10. S. B. Levy, *J. Appl. Microbiol.* **92**, 65S (2002).
11. M. C. Maiden, E. O. Davis, S. A. Baldwin, D. C. Moore, P. J. Henderson, *Nature* **325**, 641 (1987).
12. T. Hirai *et al.*, *Nature Struct. Biol.* **9**, 597 (2002).
13. T. Hirai, J. A. Heymann, P. C. Maloney, S. Subramaniam, *J. Bacteriol.* **185**, 1712 (2003).
14. W. P. Jencks, *Adv. Enzymol. Relat. Areas Mol. Biol.* **51**, 75 (1980).
15. C. Tanford, *Annu. Rev. Biochem.* **52**, 379 (1983).
16. I. C. West, *Biochim. Biophys. Acta* **1331**, 213(1997).
17. G. Chang, R. H. Spencer, A. T. Lee, M. T. Barclay, D. C. Rees, *Science* **282**, 2220 (1998).
18. D. A. Doyle *et al.*, *Science* **280**, 69 (1998).
19. M. J. Lemieux *et al.*, in preparation.
20. C. O. Rock, J. E. Cronan, in *Biochemistry of Lipids and Membranes*, D. E. Vance, J. E. Vance, Eds. (Benjamin/Cummings, Menlo Park, CA, 1985), p. 73.
21. C. M. Elvin, C. M. Hardy, H. Rosenberg, *J. Bacteriol.* **161**, 1054 (1985).
22. S. Hayashi, J. P. Koch, E. C. C. Lin, *J. Biol. Chem.* **239**, 3098 (1964).
23. S. V. Ambudkar, T. J. Larson, P. C. Maloney, *J. Biol. Chem.* **261**, 9083 (1986).
24. M. Auer *et al.*, *Biochemistry* **40**, 6628 (2001).
25. P. C. Maloney, S. V. Ambudkar, V. Anatharam, L. A. Sonna, A. Varadhachary, *Microbiol. Rev.* **54**, 1 (1990).
26. Materials and methods are available as supporting materials on *Science* Online.
27. P. Gött, W. Boos, *Mol. Microbiol.* **2**, 655 (1988).
28. H. Sui, B. G. Han, J. K. Lee, P. Walian, B. K. Jap, *Nature* **414**, 872 (2001).
29. R. Dutzler, E. B. Campbell, M. Cadene, B. T. Chait, R. MacKinnon, *Nature* **415**, 287 (2002).
30. K. P. Locher, A. T. Lee, D. C. Rees, *Science* **296**, 1091 (2002).
31. M. Sato, M. Mueckler, *J. Biol. Chem.* **274**, 24721 (1999).
32. S. V. Ambudkar, V. Anantharam, P. C. Maloney, *J. Biol. Chem.* **265**, 12287 (1990).
33. A. K. Chamberlain, S. Faham, S. Yohannan, J. U. Bowie, *Adv. Protein Chem.* **63**, 19 (2003).
34. J. F. Riordan, *Mol. Cell. Biochem.* **26**, 71 (1979).
35. M. C. Fann *et al.*, *J. Membr. Biol.* **164**, 187 (1998).
36. T. E. Creighton, *Proteins: Structures and Molecular Properties* (Freeman, New York, 1983), p. 137.
37. M. Matos, M. C. Fann, R. T. Yan, P. C. Maloney, *J. Biol. Chem.* **271**, 18571 (1996).
38. M. C. Fann, P. C. Maloney, *J. Biol. Chem.* **273**, 33735 (1998).
39. A. E. Jessen-Marshall, R. J. Brooker, *J. Biol. Chem.* **271**, 1400 (1996).
40. J. J. Chin, E. K. Jung, C. Y. Jung, *J. Biol. Chem.* **261**, 7101 (1986).
41. E. K. Jung, J. J. Chin, C. Y. Jung, *J. Biol. Chem.* **261**, 9155 (1986).
42. T. Asano *et al.*, *FEBS Lett.* **298**, 129 (1992).
43. A. L. Green, E. J. Anderson, R. J. Brooker, *J. Biol. Chem.* **275**, 23240 (2000).
44. S. G. Olsen, K. M. Greene, R. J. Brooker, *J. Bacteriol.* **175**, 6269 (1993).
45. J. A. Hall, M. C. Fann, P. C. Maloney, *J. Biol. Chem.* **274**, 6148 (1999).
46. http://pymol.sourceforge.net/.
47. A. Nicholls, K. A. Sharp, B. Honig, *Proteins* **11**, 281 (1991).

48. We are grateful to M. Becker (National Synchrotron Light Source, Brookhaven National Laboratory) and F. Rotella (Advanced Proton Source, Argonne National Laboratory) for assistance in x-ray diffraction experiments; M. T. Pope for the gift of tungsten clusters; R. MacKinnon and H. Sui for advice on crystallography; and Y. Lu and T. Neubert for mass spectrometry measurements. We thank R. Goetz, L. Kanbi, and M. Safferling for participating in synchrotron trips and J. Belasco, H. Griffith, S. Hubbard, X. P. Kong, X. D. Li, R. Reithmeier, and D. Stokes for helpful discussion and critical reading of the manuscript. M.A. thanks the Human Frontier Science Program and the Agouron Institute–Jane Coffin Childs Memorial Fund for postdoctoral fellowships. This work was financially supported by NIH and by the Diabetes Research Bridging Fund of the New York State Department of Health. Atomic coordinates have been deposited with the Protein Data Bank under access code 1PW4. The authors dedicate this work to the memory of Dr. Matti Saraste.

Supporting Online Materials

www.sciencemag.org/cgi/content/full/301/5633/616/DC1
Materials and Methods
Figs. S1 to S4
Movies S1 and S2
References

4 June 2003; accepted 3 July 2003